Support Condition Monitoring of Offshore Wind Turbines Using Model Updating Techniques

Ying Xu[1], George Nikitas[2], Tong Zhang[3], Qinghua Han[1], Marios Chryssanthopoulos[2], Subhamoy Bhattacharya[2], Ying Wang[2, *]

1. Key Laboratory of Earthquake Engineering Simulation and Seismic Resilience of China Earthquake Administration, Tianjin University, Tianjin 300350, China.

2. Department of Civil and Environmental Engineering, University of Surrey, Guildford, Surrey GU2 7XH, the United Kingdom

3. School of Biomedical Engineering and Imaging Science, Kings College London, London, SE1 7EU, the United Kingdom

Abstract

The offshore wind turbines (OWTs) are dynamically sensitive, whose fundamental frequency can be very close to the forcing frequencies activated by the environmental and turbine loads. Minor changes of support conditions may lead to the shift of natural frequencies, and this could be disastrous if resonance happens. To monitor the support conditions and thus to enhance the safety of OWTs, a model updating method is developed in this study. A hybrid sensing system was fabricated and set up in the laboratory to investigate the long-term dynamic behaviour of the OWT system with monopile foundation in sandy deposits. A finite element (FE) model was constructed to simulate structural behaviours of the OWT system. Distributed nonlinear springs and a roller boundary condition are used to model the soil-structure-interaction (SSI) properties. The FE model and the test results were used to analyze the variation of the support condition of the monopile, through an FE model updating process using Estimation of Distribution Algorithms (EDAs). The results show that the fundamental frequency of the test model increases after a period under cyclic loading, which is attributed to the compaction of the surrounding sand instead of local damage of the structure. The hybrid sensing system is reliable to detect both the acceleration and strain responses of the OWT model and can be potentially applied to the remote monitoring of real OWTs. The EDAs based model updating technique is demonstrated to be successful for the support condition monitoring of the OWT system, which is potentially useful for other model updating and condition monitoring applications.

Keywords: Offshore wind turbines, Monopile, Sand, Model updating, Estimation of Distribution Algorithms

1. Introduction

In recent years, a great number of Offshore Wind Turbines (OWTs) were constructed around the world to reduce energy pressure and improve the ecological environment in coastal areas. The typical foundations of OWTs include monopile, gravity base, jacket, suction caisson and floating system [1], etc. Among all these kinds of foundations, the monopile is most widely used due to its simplicity [2]. However, it has been confirmed that the monopile OWTs are dynamically sensitive structures, especially the "soft-stiff" ones, whose fundamental frequencies are fixed in a very narrow range between the rotor frequencies f_{1P} (0.135-0.316Hz) and the blade passing frequencies f_{3P} (0.405-0.948Hz) [3-5]. Under dynamic loading, the soil will interact with the OWTs, which may lead to an inevitable change of the soil stiffness. This change may shift the fundamental frequency of the OWT system to the forcing frequency zones (f_{1P} or f_{3P}), which may result in unwanted resonance and should be avoided [6]. The above conclusions have been confirmed by the analysis of ten case studies in [5]. Therefore, an accurate evaluation of the fundamental frequency and investigation of the long-term dynamic behaviour of the OWT systems are of great importance to ensure their safe operation.

A series of experimental studies were carried out to reveal the long-term dynamic performance of monopile OWTs. Firstly, the scaling laws of the test model related to the dynamic responses of the OWTs were studied thoroughly by Bhattacharya et al [2, 7]. Among these studies, considerable work focused on identifying the changes in soil stiffness during the soil-structure interaction. In most studies, the stiffness of the soil was simulated by the "*p-y*" method according to the API code [8], although some researchers noted that the API model may lead to the overestimation of pile-soil stiffness [2, 9]. Secondly, many research efforts are placed on the establishment and improvement of the soil-structure interaction (SSI) model for finite element analysis (FEA), based on the test results [10-13]. Many kinds of nonlinear spring models were proposed to simulate the dynamic soil-structure interaction: distributed spring model [9, 11], three-spring model (lateral spring, rotational spring and vertical spring [12], four-spring model (lateral spring, rotational spring, rotational-lateral coupled spring and vertical spring) [2, 5] and simplified lumped mass SDOF model [13]. Based on the scaled model test and the FEA results, the following conclusion was drawn: long-term cyclic loading may cause either stiffening or softening of the soil around the pile foundation of an OWT, i.e. stiffening for the sandy soil [14-19] and softening for the clayey soil [2, 3, 20].

Structural Health Monitoring (SHM) has been recognized internationally as an effective way to enhance structural reliability and resilience, which enables the assessment of structural conditions and early detection of potential component failures [21]. In recent years, SHM technology has been gradually applied to the OWTs. Long-term dynamic monitoring on an OWT in the Belgian North Sea was conducted to evaluate the vibration levels and modal parameters of the fundamental modes of the support structure [22]. A foundation SHM strategy for

monopiles was developed and applied to an operational OWT [23]. The long-term monitoring results confirm the earlier observation that the turbine becomes stiffer in the monitoring period. Meanwhile, low-cost wireless sensors became an enabling technology for conditional monitoring of operating OWTs. It's demonstrated that the wireless sensors, with their inherent on-board data processing abilities, can be used to automate monitoring and damage detection in large-scale wind turbines in an economical manner [24-26]. In addition, a series of damage localization methods and statistical pattern recognition paradigm for SHM of OWT were discussed in such research papers as [27] and [28]. However, most of the present research focuses on the behaviour of the structure or the mechanical system, instead of the whole OWT system with soil supports.
In this paper, the long-term dynamic behaviour of OWT with monopile foundation in the sandy deposits is studied based on model test and FE analysis. An innovative hybrid sensing system, with acceleration and strain monitoring capacities, is developed to simulate the remote sensing of the real OWTs in extreme environments. An FE model is constructed and the Estimation of Distribution Algorithms (EDAs) is used to evaluate the variation of the support conditions of the OWT system through a model updating process [29-30].

2. Experimental investigation on a monopile OWT

2.1 The laboratory model

The tests were carried out in the Surrey Advanced Geotechnical Engineering (SAGE) laboratory in the University of Surrey, UK. As shown in Fig.1, the monopile OWT model consists of four parts: the monopile and the tower made of aluminium alloy; the connection parts fastened by four bolts; and the top mass representing the assembly of the nacelle, rotor hub, and blades. The parameters of the OWT model are summarized in Table 1. The dimension of the container is 1,200mm long, 1,000mm wide, and 600mm deep. The soil used in the test is the Red Hill silica sand, with a 500mm depth in the tank. The basic properties of the sand are listed in Table 2.

In the model design, the dynamic scaling laws of the OWT model were first determined to simulate and predict the long-term behaviour of the prototype. To describe the similitude relationships, four dimensionless variables were considered in this work [2, 7]: (1) Ratio of length to diameter (L/D, where L is the tower length and D is the pile diameter), which reflects the geometry and stiffness of the pile. (2) Cyclic stress ratio (CSR), which affects the strains and stiffness of the surrounding soil, and is represented by the non-dimensional variable (P/GD^2, where P is the total equivalent horizontal load and G is the shear modulus of soil, or M/GD^3, where M is the overturning moment at the ground level). (3) Ratio of the loading frequency to the system frequency (f_f/f_n), which satisfies the dynamic response similarities between the model and the prototype. (4) Rate of loading, which influences the generation and dissipation of pore pressure, and is represented by ($k_h/f_f D$, where k_h is the horizontal permeability of soil).

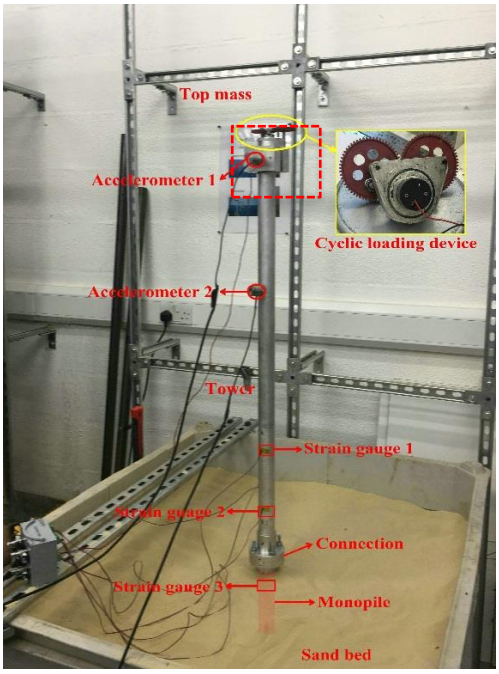

Fig. 1 Setup of the OWT model test.

Table 1 Detailed parameters of the OWT model.

Component	Length (cm)	Diameter (cm)	Thickness (mm)	Mass (g)
Model pile	35	4.1	0.75	777
Model tower	100	4.1	0.75	261
Top mass	--	--	--	824

Table 2 Properties of the Red Hill silica sand.

Properties	Values
Specific gravity G_s	2.65
Median particle diameter D_{50} (mm)	0.12
Internal friction angle ϕ (deg)	36.0
Dry unit weight γ_d (kN/m^3)	16.8
Maximum void ratio e_{max}	1.037
Minimum void ratio e_{min}	0.547
Relative density D_r	0.63
Shear modulus G (MPa)	10.0
Uniformity coefficient C_u	1.63
Horizontal permeability k_h (m/s)	10^{-4}

The properties of the OWT model were compared with another monopile model test [14] and a prototype in similar soil conditions [17], as shown in Table 3. The dimensionless similitude relationships for models and prototype are listed in Table 4. It can be seen that the dimensionless variables of the scaled model are basically in accordance with the prototype, to ensure that the long-term dynamic behaviour of the OWT model can reflect that of the prototype realistically.

Table 3 Properties of monopile and soil profile for physical model and prototypes.

	Properties	Physical model in this paper	Physical model in [14]	Prototype in [17]
Tower & Monopile	Material	Aluminium alloy	Steel	Steel
	Diameter of monopile D (m)	0.041	0.043	5
	Length of monopile h (m)	0.350	0.450	20
	Thickness of monopile t (cm)	0.075	0.020	5
	Height of tower L (m)	1.0	1.0	90
Soil profile	Type	Sand	Sand	Sand
	Shear modulus G (MPa)	10	10	100
	Horizontal permeability k_h (m/s)	10^{-4}	10^{-4}	5×10^{-4}
	Internal friction angle ϕ (deg)	36.0	36.0	35.5
Horizontal loads	P (MN)	1.0×10^{-6}	$(0.5\text{-}4.7)\times10^{-6}$	1.0

Table 4 Dimensionless groups for models and prototype.

Dimensionless variables	Physical model in this paper	Physical model in [14]	Prototype in [17]
L/D	24.39	23.26	18
$P/GD^2(\times 10^{-4})$	0.59	0.25-2.55	4
$k_h/f_f D(\times 10^{-4})$	2.44	1.63	4.12
f_f/f_n	1.51	0.85/1.30	2.06

2.2 Test procedure and equipment

In this study, the laboratory test is divided into three stages. Firstly, the OWT model was placed in the container, and modal tests were conducted to determine the initial structural and support conditions. Secondly, the OWT model was continuously excited by a cyclic loading system until the strain and acceleration responses became stable. In this study, the total cycle number N was 8.8×10^5. Thirdly, modal tests were conducted again on the OWT model, to investigate the change of the structural and support conditions after a long period of cyclic loading. The first and third stages of the test are referred to as modal test in the rest of the paper, while the second stage of the test is referred to as cyclic loading test.

The schematic diagram of the simplified OWT model used in the test is shown in Fig.2. Two unidirectional accelerometers (in x-direction) were installed on the model tower to investigate the vibration characteristics of the system. Three pairs of strain gauges were attached to the tower and the monopile to obtain the local stress/strain responses of the model. The locations of the accelerometers and strain gauges were determined according to the FE results. The accelerometers were located at the positions with larger displacement mode shape, and the strain gauges were arranged at the positions with higher stress level.

A sensing system manufactured by Zhixing Technologies was used during the whole test, as shown in Fig. 3. Traditional strain gauges and accelerometers are connected to a multi-sensor wireless node in this sensing system, which can transmit the data to the base station wirelessly using the Zigbee protocol. Such a kind of system realizes the wireless sensing function by using the wireless nodes with traditional sensors and thus is named as a hybrid sensing system. The sensitivity and frequency range of the selected accelerometers are 150mV/ms^{-2} and 0.2-1500 Hz, respectively. The type of the strain gauges is the normal 120Ω one, with a quarter bridge configuration. The sampling frequency is 100Hz for the modal tests and 50Hz for the cyclic loading test. All the data were collected by the multi-sensor wireless node and transmitted wirelessly to the base station about 30 meters away, which attempted to simulate the remote sensing in the real field. This distance can be up to 500 meters if there is no block between the base station and wireless node.

It should be noted that in this laboratory test, unidirectional accelerometers were used since the excitation is unidirectional as well. In practices, tri-axial accelerometers may be essential to obtain the vibration responses of the OWTs in all three directions.

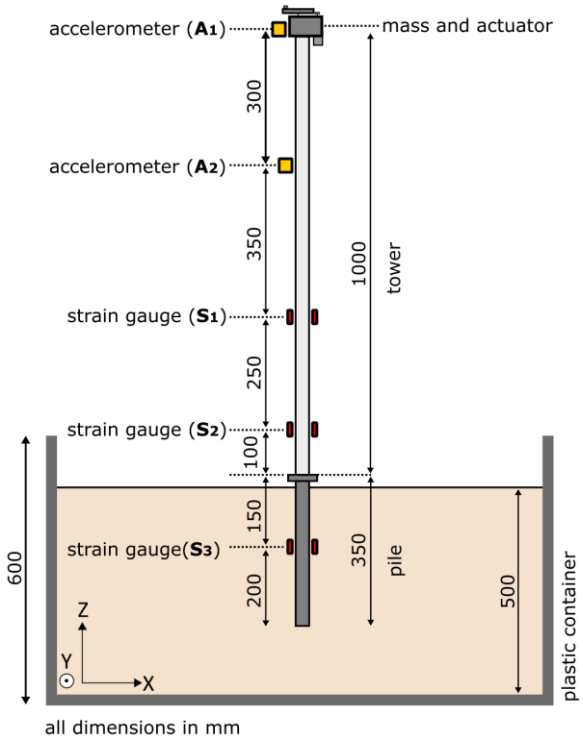

Fig.2 Schematic diagram of simplified OWT model.

To provide loads in the cyclic loading test, a balance gear system was attached at the top of the monopile model [14], as shown in Fig.1. The direction and amplitude of the cyclic loads are controlled by the values of the two out-of-balance masses in the gear system. The loading frequency is controlled by the input voltage. In this

test, one-directional two-way cyclic load was applied to simulate the combination of wind, wave and current loads in real applications, as shown in Fig. 4. The amplitude and frequency of the cyclic load are provided as $1N$ and 10Hz, respectively. This aims to achieve a similar f_f/f_n ratio as that of the prototype and a reasonable strain level in the structure. Since this paper mainly focuses on the monitoring of support conditions of the OWT system, the cyclic load is designed to be small enough to avoid fatigue or strength failure of the structure. Further details regarding the cyclic loading device and the parameter settings can be found in [2], [4], and [12].

(a) Accelerometer (b) Strain signal processor (c) Multi-sensor wireless node (d) Multi-sensor wireless base station

Fig. 3 Composition of the hybrid sensing system.

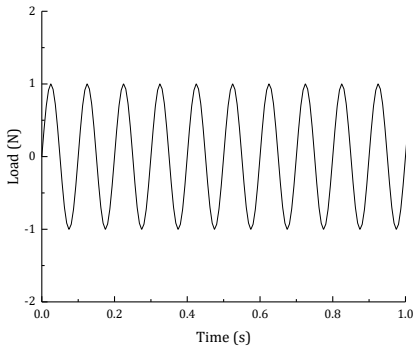

Fig.4 Cyclic load acting on the OWT model (in 1 s).

3 Test results

3.1 Modal test results

The modal tests were carried out for ten times, respectively before and after the cyclic loading test. An impact hammer with the loading capacity of 4.45kN was used in the modal tests to generate impact loads, and the vibration signals of the OWT model including both accelerations and strains were recorded by the hybrid sensing system. Fig.5 shows the typical acceleration time histories during the modal tests. Compared with the acceleration response obtained from A1, the amplitude of acceleration obtained from A2 increased dramatically in the later stage of free vibration, as shown in Fig.5(a). Since this phenomenon occurred in every modal test before the cyclic loading test, it is not due to the error of testing. The potential reason is the vibration nonlinear effect caused by the compaction of soil. To understand this, we generated the spectrograms for both accelerometers

in the modal tests. As can be seen in Figs. 6 and 7, the structural responses are generally stationary with small variations. In Fig. 6, there is clearly some low-frequency energy in the spectrogram for A2 before cyclic loading, while for A1, the energy (or amplitude) for this frequency is close to zero. In comparison, Fig.7 shows that after cyclic loading, this energy in A2 is much lower than that before cyclic loading. This can partly explain the existence of additional vibration in Fig.5(a). To fully understand this effect, more rigorous tests and analysis are needed in future studies.

The modal analysis of the OWT model before and after the cyclic loading test was conducted by using Welch's method [31], based on the acceleration data. The distributions of the power spectral amplitude in the frequency domain are shown in Fig.8. It is observed that the fundamental frequencies obtained from two accelerometers are consistent with each other, both equal to 6.64Hz before the cyclic loading test, and increasing to 7.28Hz after the test. Meanwhile, the power spectral amplitudes became more than two times after the cyclic loading test. All these indicate that the soil stiffness increased after a period of vibration.

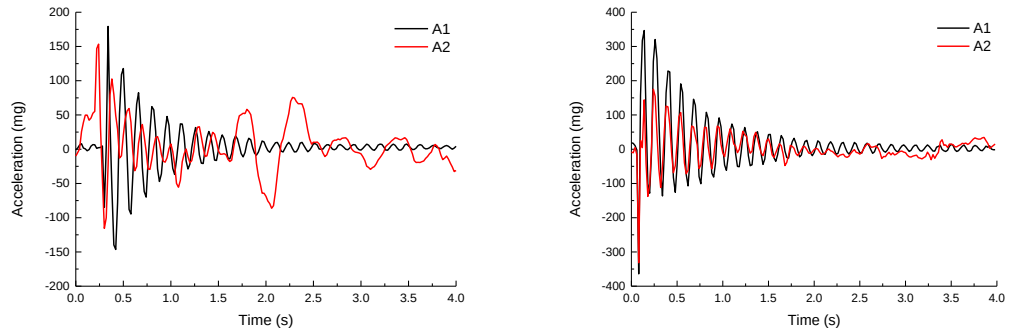

(a) Before the cyclic loading test (b) After the cyclic loading test

Fig.5 Acceleration time histories before and after the cyclic loading test.

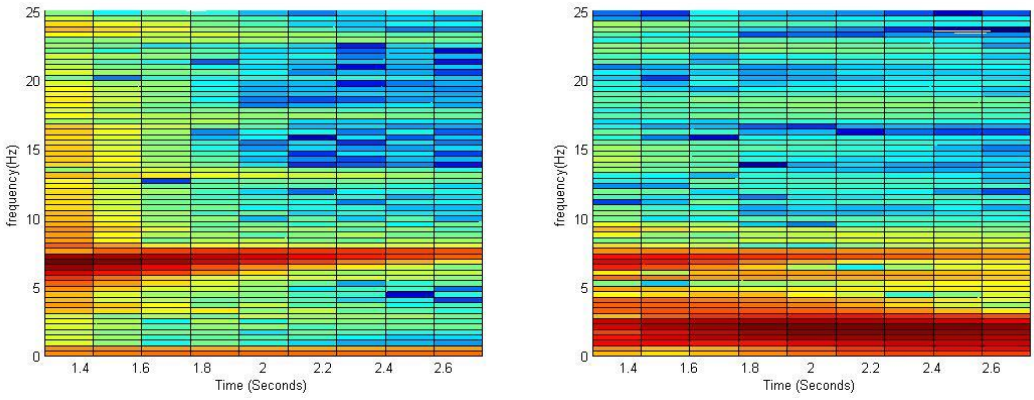

(a) A1 (b) A2

Fig.6 Spectrogram for modal test before cyclic loading test

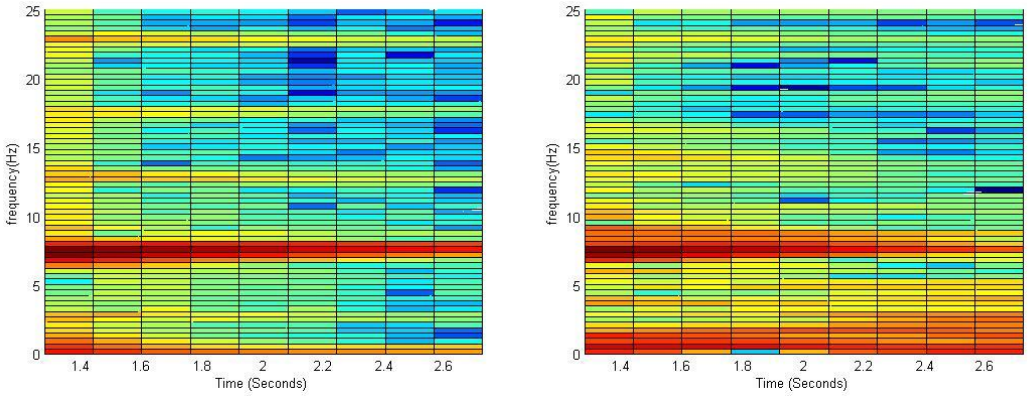

(a) A1 (b) A2

Fig.7 Spectrogram for modal test after cyclic loading test

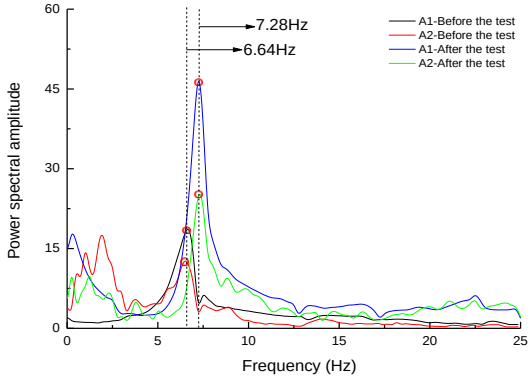

Fig.8 Modal analysis results by using Welch's method.

Table 5 Modal analysis results based on ARTeMIS Modal software.

	Before the cyclic loading test		After the cyclic loading test	
	FDD	EFDD	FDD	EFDD
Natural frequency	6.909	6.541	6.982	6.872
Damping ratio	--	7.865%	--	7.343%
Mode shape at $7/10L$	0.5429	0.6127	0.5213	0.5016
Mode shape at L	0.8398	0.7903	0.8534	0.8651

Note: FDD-Frequency domain decomposition; EFDD-Enhanced frequency domain decomposition.

For comparison, the modal analysis of the OWT model was also carried out by using commercial software, ARTeMIS Modal [32], which is regarded as a high-quality modal analysis tool. The fundamental frequency, damping ratio, as well as the mode shape were obtained and shown in Table 5. The difference between the natural frequencies obtained by using Welch's method and ARTeMIS is less than 4.0%, which confirmed the validity of the modal analysis results in this study.

The test and modal analysis results clearly show that the fundamental frequency of the laboratory OWT model increased by 9.6% after a period of continuous cyclic loading. In reality, the change of the fundamental frequency of a structure may lead to disastrous situations when it moves into the forcing frequency zone. Although the percentage change cannot be scaled to the real structures, this clearly shows the necessity of SHM for the safe operation of OWTs. In order to determine the exact support condition, FE model updating is performed in this study, which will be presented in Section 4.

It should be noted that there are mainly three excitation methods for modal tests, i.e. impact hammer, shaker, and ambient vibration. In the laboratory, the performances of the three methods are very similar, while the impact hammer test is the most straightforward and effective way. Since this research mainly focuses on the verification of the model updating technique and the exploration of the hybrid sensing system for conditional monitoring of OWTs, the impact hammer excitation method was adopted. As for the real turbines subject to ambient excitation, the modal parameters can be obtained through operational modal analysis (OMA).

3.2 Cyclic loading test results

The acceleration and strain responses of the OWT model are recorded by the hybrid sensing system during the cyclic loading test. The test data was saved in the computer automatically every half hour. Since the structural responses changed very slowly during the cyclic loading test, the acceleration amplitudes and the median stresses corresponding to every 10^5 cycles are extracted, as shown in Fig.9. Meanwhile, three typical time histories of acceleration and stress responses at the end of N=2×10^5, 5×10^5 and 8×10^5 are shown in Figs. 10 and 11, respectively.

Fig.9 (a) shows the variation of acceleration amplitude with respect to the cyclic number. At the beginning of the cyclic loading test, the amplitudes of acceleration increase sharply with the cycle number until N=2×10^5. Then, the acceleration amplitudes decrease gradually with the increase of the cycle number. After a period of fluctuation, the acceleration amplitudes reduce to a level at around 2,000mg in the second half of the cyclic loading test.

The influencing factors of the acceleration amplitudes include the loading amplitude, boundary conditions (soil restraint) and the structural stiffness. Firstly, since the loading amplitude kept constant at a low level in the whole loading process, it is not considered as influencing in this study. Secondly, referring to the fatigue design curves for 6061-T6 Aluminum [33], fatigue failure cannot occur to aluminum structures when the stress level is lower than 10Mpa, even with 10^9 number of cycles. Since this paper mainly focuses on the monitoring of soil conditions instead of structural damage, the cyclic load in our test is designed to be small enough to avoid fatigue or strength failure of the structure (the stress level is less than 4,200 Pa according to the test results). This is further confirmed by the fact that no crack or bolt loosening was observed during and after the test.

Therefore, the change of the structural stiffness is not considered as influencing. Based on the above, the decrease of the acceleration amplitudes is mainly caused by the change of the soil stiffness.

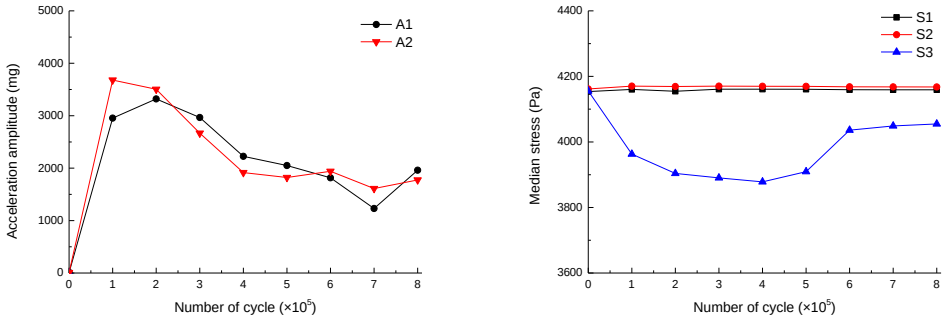

(a) Variation of the acceleration amplitude (b) Variation of the median stress

Fig.9 Variation of structural responses during the cyclic loading test

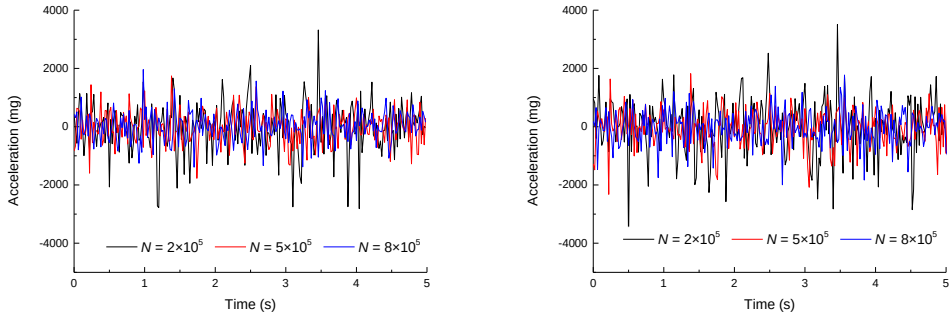

(a) A1 (b) A2

Fig.10 Acceleration time histories during the cyclic loading test.

Fig.9 (b) shows the variation of stress amplitudes (calculated based on strain recordings) with respect to the cycle number. It is noted that the values of stress at S1 and S2 (on the tower) remains constant in the loading process. By contrast, the value of stress at S3 (on the monopile) decreases dramatically from 4,200Pa to less than 4,000pa at around N=1-2×10^5, then stabilize at around 3,900Pa until N=5×10^5, and returns to 4050Pa after N=6×10^5. Fig.11 clearly shows that the variations of stress amplitude at S1 and S2 are quite small during the cyclic loading test, i.e. less than 20Pa for all the measuring points; however, the variation of those at S3 is much larger. It indicates that the strains on the monopile are very sensitive to the change of stiffness of the surrounding soil. In future studies, it is suggested to use a distributed strain monitoring strategy, e.g. fibre optical sensors.

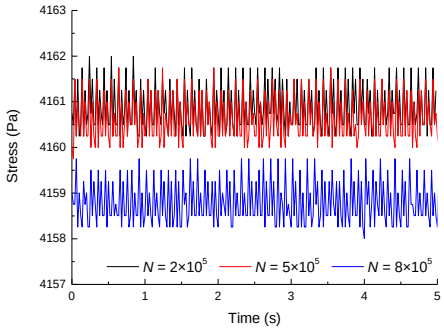

(a) S1

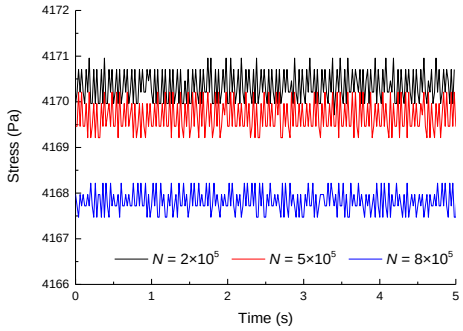

(b) S2

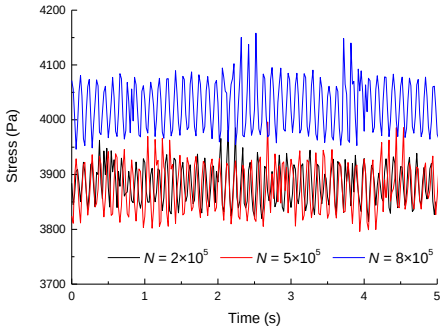

(c) S3

Fig.11 Stress time histories during the cyclic loading test.

4 Model updating and validating

4.1 Tactic of model updating

In civil engineering domain, the numerical method, especially FEA, is commonly used for structural design and evaluation. However, a great difference may exist between the numerical results and real structural responses, due to the simplification and/or idealization of the geometric parameters, constitutive model and boundary conditions. To solve this problem, the FE model updating technique can be used to calibrate the numerical model. Furthermore, the FE model updating technique can also realize structural condition identification within SHM domain. Therefore, the process of model updating is normally divided into two stages: 1) Calibration of the FE model based on the responses from the intact structure, and 2) Further updating of the FE model based on the responses from the damaged structure.

Model updating is a typical optimization process, which includes three key components: updating parameters, objective functions and optimization algorithm. The updating parameters are usually the unknown/uncertain variables (i.e. stiffness, cross-sectional area and Young's modulus, etc.). After updating, the parameter values can either determine the values of uncertain variables or reflect the change of structural conditions, i.e. damage location and severity. The objective function is normally derived from damage-sensitive features, such as

modal parameters. Thus, FE model updating process can be summarized as follows: by evaluating damage-sensitive features from both numerical and test results, the corresponding parameters within the FE model are updated to suit the test results better by minimizing the value of objective functions using an optimization algorithm.

In this paper, the model updating technique is realized by using an evolutionary optimization algorithm, EDAs [34]. The EDAs based model updating mainly includes four parts: selection based on the objective function, learning and sampling to generate new individuals in the next generation, replacement of the ineffective individuals. Compared with classical genetic algorithms, learning and sampling are realized based on probabilistic models in EDAs, which makes the optimization process more efficient and flexible. Therefore, EDAs can provide not only the optimal updating parameters but also the probability distribution of the parameters, e.g. the variance. This can further provide the confidence level of the updated results, which is not commonly available in other optimization algorithms.

In this study, the Gaussian Network model is selected as the probabilistic model due to its popularity in this kind of problems. The variation of the soil support conditions is selected as the updating parameters. Two objective functions are selected in model updating [29]:

$$J_1 = \sum_{i=1}^{m}\left(\frac{f_{ai}-f_{ei}}{f_{ei}}\right)^2 \tag{1}$$

$$J_2 = \sum_{i=1}^{m}\sum_{j=1}^{m}\left(\frac{\boldsymbol{\Phi}_{ai}\cdot\boldsymbol{\Phi}_{aj}}{f_{ai}^2} - \frac{\boldsymbol{\Phi}_{ei}\cdot\boldsymbol{\Phi}_{ej}}{f_{ei}^2}\right)^2 \tag{2}$$

where f_i represents the i^{th} natural frequency; *a* and *e* represent analytical and experimental results respectively; *m* is the number of modes; $\boldsymbol{\Phi}_i$ and $\boldsymbol{\Phi}_j$ are the i^{th} and j^{th} modal shapes, respectively. The model updating process will be completed when J_1 or J_2 converges to zero. Otherwise, the updating process will be governed by J_1 until reaching the specified generation.

4.2 The nonlinear p-y model used in FE analysis

As recommended in API standard [8], *p-y*, *t-z* and *q-z* curves are used to represent the soil resistances in the horizontal and vertical directions. Since the main load acting on the OWT model is the lateral load, *p-y* curve plays a dominant role. Therefore, only the nonlinear *p-y* model is considered in this paper, which can be described as [8]:

$$p = Ap_r \cdot \tanh\left(\frac{kz}{Ap_r}\cdot y\right) \tag{3}$$

where *A* is the factor to account for cyclic or static loading condition, evaluated by:

$$A = 0.9 \qquad \text{for cyclic loading} \tag{4}$$

$$A = (3.0 - 0.8\frac{z}{D}) \geq 0.9 \qquad \text{for static loading} \tag{5}$$

k is the initial modulus of subgrade reaction (kN/m^3), y is the lateral deflection (m), and D is the average pile diameter (m). p_r is the representative lateral capacity at depth z (kN/m), which is calculated as follows:

$$p_{rs} = (C_1 z + C_2 D)\gamma z \tag{6}$$

$$p_{rd} = C_3 D \gamma z \tag{7}$$

$$p_r = \min(p_{rs}, p_{rd}) \tag{8}$$

where p_{rs} and p_{rd} are the lateral capacities of soil (kN/m) corresponding to the shallow depth and deep depth, respectively; γ is the unit weight of soil (kN/m^3); C_1, C_2, and C_3 are coefficients dependent on the angle of internal friction ϕ.

The values of C_1, C_2, C_3 and k are determined by the properties of sand, as listed in Table 6. Substituting the above parameters into Eq. (3) to Eq. (8), then the *p-y* curves corresponding to different soil depth z could be obtained.

Table 6 Parameters related to the *p-y* curves.

Parameter	Value	Unit
A	0.9	-
C_1	3.1	-
C_2	3.6	-
C_3	60	-
D	4.1	cm
k	43.4	MN/m^3
γ	16.8	kN/m^3

4.3 FE model of the monopile OWTs

The FE model of the monopile OWT is established in ANSYS 12.1, as shown in Fig.12. The tower and monopile are both simulated by Element Beam 188. A roller boundary condition is introduced at the end of the monopile [9]. The material properties of the FE model are shown in Table 7. The top mass, the accelerometer mass and the connection mass are taken as 824g, 140g and 694g respectively, which are all simulated by Element Mass 21. The buried depth of the monopile d is 32.8cm, which is in accordance with the measured value in the test. Considering the length of the monopile model (less than 0.4m), four horizontal springs are accurate enough to simulate the interaction between the soil and the OWT model. One nonlinear spring at the bottom of the monopile as well as another three springs with uniform spacing of $d/3$ (Combine 39) were introduced in the FE model. The spacing between the soil surface and the top spring, and that between the third spring and the bottom spring were set to be equal. The stiffness of the springs is determined according to the nonlinear *p-y* model of sand, which varies with the depth z, as shown in Fig. 13.

Based on the test results shown in Table 5, the damping ratio of the OWT model is constant (changed less than 7% after the cyclic loading test). Further, the damping

of soil is a secondary influencing factor of structural frequency change, and thus the damping ratio is simulated as a constant of 7.5% in the FEA.

It should be noted that soil behaviours are very complex. A more refined FE model could deliver more accurate results. However, as shown in previous studies [35, 36], the simplified spring model for soil supports is capable of structural condition identification. Thus, in this study, the simplified FE model is adopted.

4.4 Model updating based on the EDAs

For the FE model in Fig.12, the changeable parameters during the model updating are the stiffness parameters of the four springs. Therefore, the values of K_1, K_2, K_3 and K_4 are selected as the updating parameters. The reaction force of each spring equals the lateral capacity of sand with a certain depth (d/6 to d/3). The stiffness of each spring is determined by the secant slope of the *p-y* curve. According to Fig.13, the original values of the spring stiffness, from bottom to top are set as 2.7×10^5 N/m, 2.6×10^5 N/m, 2.1×10^5 N/m, 8.8×10^4 N/m, respectively.

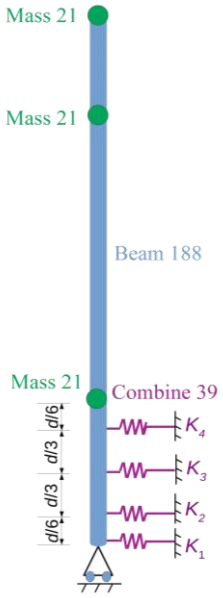

Fig.12 FE model established in ANSYS.

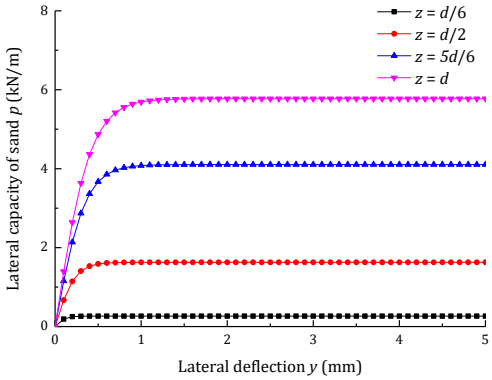

Fig.13 The nonlinear *p-y* model of sand.

Table 7 Material properties of the FE model.

Material	Young's modulus	Poisson ratio	Yield Strength	Density
Aluminium alloy	70GPa	0.3	210MPa	2700kg/m^3

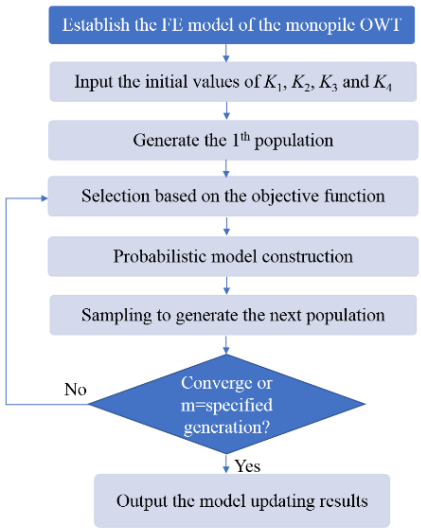

Fig.14 Flowchart of the EDA based model updating.

After that, the selected parameters (K_1, K_2, K_3, K_4) are updated by using the EDAs, through the process shown in Fig.14. The model updating was carried out two times. The first model updating was performed for minimizing the difference between the FE model and the test model. The second model updating was performed to evaluate the change of soil stiffness after the cyclic loading test.

The natural frequency and mode shape obtained from the FE model before and after the model updating are compared with the test results, as shown in Table 8. It is noted that the error of the natural frequency between the test result and that obtained from the initial FE model is less than 1.7%, which demonstrates the validity of the FE model.

Table 8 Comparison of the modal analysis results.

	Before the cyclic loading test			After the cyclic loading test	
	FEA (initial)	FEA (First update)	Test result	FEA (Second update)	Test result
Natural frequency	6.431	6.541	6.541	6.872	6.872
Mode shape at $7/10L$	0.571	0.561	0.613	0.535	0.502
Mode shape at L	0.870	0.860	0.790	0.832	0.865

To better describe the change of the updating parameters, the parameters f_1, f_2, f_3 and f_4 are introduced, which is the ratio of the updated value to the initial value.

In the first model updating, the updating factors quickly converged after the 6th generation, as shown in Fig.15 (a), and Table 9. Further, the variance values of the updating factors among different generations are presented in Fig.15 (b). It is shown that the variance values decline to 10^{-7} after the 6th generation, which demonstrates that the updating results are very stable. Compared with other model updating algorithms, the EDAs-based model updating method can provide

the quantification of uncertainty of the updating parameters, in addition to the updated parameters. Therefore, it provides further confidence in using the updating results.

After the first model updating, the natural frequency obtained from the FE model is very close to the test result. Thus, the updated numerical model is considered to be accurate enough to simulate the structural behaviour of the OWT system. The stiffness of springs is corrected as 3.2×10^5 N/m, 2.7×10^5 N/m, 2.2×10^5 N/m, 9.6×10^4 N/m, respectively. Compared with the original values assumed from the *p-y* curve, the changes of K_2 and K_3 are less than 5%, while those of K_1 and K_4 are around 10%. This demonstrates that the use of the *p-y* curve to determine initial soil stiffness values is successful.

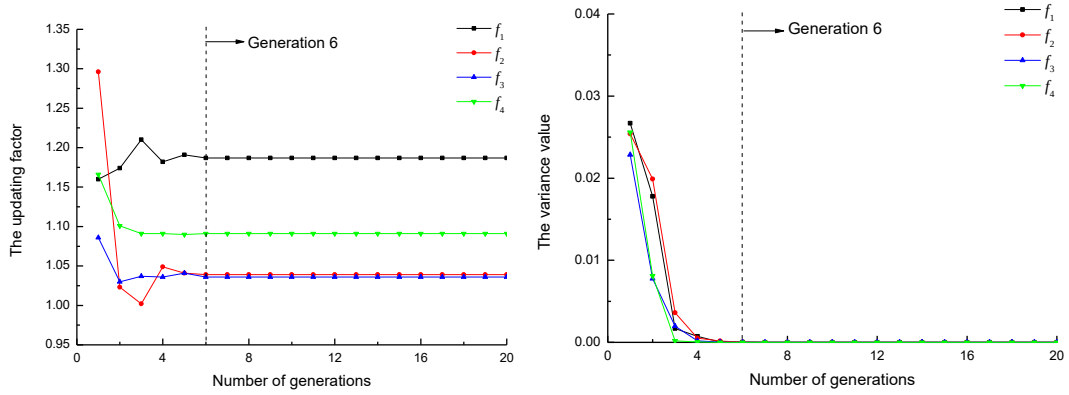

(a) The updating factors (b) The variance value

Fig.15 Performance of EDAs based model updating (First updating).

Table 9 Updating factors during the first model updating.

	$f_1=K_1'/K_1$	$f_2=K_2'/K_2$	$f_3=K_3'/K_3$	$f_4=K_4'/K_4$
Generation 1	1.16	1.296	1.086	1.166
Generation 6	1.187	1.039	1.036	1.091
Generation 100	1.187	1.039	1.036	1.091

The second model updating results are shown in Table 10 and Fig.16. The updating factors converged after 30 generations, and the variance values of the updating factors are less than 10^{-4} after the 30th generation, which shows the reliability and stability of the updating results.

After the second model updating, the natural frequency obtained from FEA is consistent with the test result. It can be considered that the updated numerical model can reflect the real condition of the OWT test model. The spring stiffness K_4 and K_3 increased to 3.2×10^5 N/m and 2.8×10^5 N/m, respectively. Both changes are less than 10%, which demonstrates that the stiffness of both springs had only minor changes. In contrast, the values of corresponding updating factors, f_4 and f_3, are equal to 3.205 and 1.503, respectively. This indicates a large change of soil stiffness at the top half of the sandy deposits, with the increase of the top layer stiffness being more than 220%. The results demonstrate that 1) the cyclic loading

on the OWT system over a period can lead to the soil compaction; 2) the compaction is more significant at the top half of the support, with the top layer being most significant. Based on the deflection profile of the monopile, the top layer has the largest deflections under lateral loads, and thus the most significant compaction and stiffness change are expected. The level of this change is influenced by the soil density and number of cycles. Their relationship can be studied in the future.

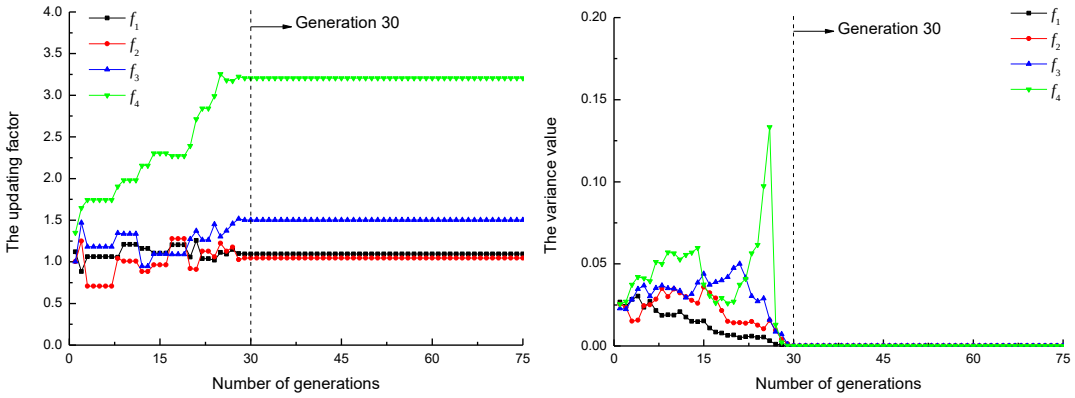

(a) The updating factor (b) The variance value

Fig.16 Performance of EDAs based model updating (Second updating).

Table 10 Updating factors during the second model updating.

	$f_1=K_1'/K_1$	$f_2=K_2'/K_2$	$f_3=K_3'/K_3$	$f_4=K_4'/K_4$
Generation 1	1.121	1.003	1.002	1.349
Generation 29	1.094	1.045	1.503	3.205
Generation 100	1.094	1.045	1.503	3.205

5. Conclusions

This paper aims to study the structural behaviour of OWT with monopile foundation in the sandy deposits over a period of vibration through an FE model updating method. A smart hybrid monitoring system was set up to evaluate the soil support condition of the OWT system before, under, and after continuous cyclic loading. The hybrid sensing system used in the test attempts to provide a remote sensing solution using traditional sensors for the real OWTs. To assess the structural and support conditions more accurately, the EDAs based model updating technique is used. Based on the experimental data and numerical results, the following conclusions can be drawn:

1. The test results indicate that the fundamental frequency of the model system increases by approximately 10% after a period of cyclic loadings. The increase of the natural frequency is attributed to the compaction of the surrounding sand instead of local damage on the tower or the monopile. However, it should be noted that the increased value cannot be scaled to predict actual changes in real OWTs.

2. During the cyclic loading test, the amplitude of acceleration initially increases as the number of cycles goes up. After reaching its peak value, the amplitude of acceleration decreases with additional cycles. Meanwhile, the value of stress on the tower remains constant in the loading process, which demonstrates that no local damage occurred to the tower during the test. By contrast, an obvious change of the stress on the monopile is observed during the cyclic loading test. The strain gauges arranged on the monopile are more sensitive to the change of stiffness of the surrounding soil.

3. The proposed FE model with distributed nonlinear springs and a roller boundary condition is applied to simulate the structural behaviour of the OWT system. The EDAs based model updating technique is used to evaluate the change of the structural and support conditions in the OWT system. The updating results demonstrate that the soil stiffness at the top layer experienced a significant increase of more than 220%, while that at the bottom half had only 10% increase, which indicates the compaction effects of cyclic loading to the soil support of the OWT system. The results confirm the effectiveness of the EDAs based model updating method for structural condition assessment in the SHM domain.

The following topics are recommended for future research efforts: 1) the development of optical fibre sensors for OWTs strain monitoring; 2) the investigation of nonlinear effects of the soil support, using refined numerical models and spectrogram; 3) the investigation of the coupled effects of OWTs under vibration with higher amplitudes which may lead to both structural fatigue damage and support condition changes.

Acknowledgement

This research was financially supported by the EPSRC Institutional Sponsorship 2016 Scheme (EP/P511456/1) and the National Natural Science Foundation of China (No. 51608360). Prof. Yan Yu is acknowledged and memorised for his remarkable contribution to the hybrid sensing system used in this work.

References

[1] Bhattacharya S. Chapter 12 – Civil Engineering Aspects of a Wind Farm and Wind Turbine Structures [J]. Wind Energy Engineering, 2017:221-242.

[2] Lombardi D, Bhattacharya S, Wood D M. Dynamic soil–structure interaction of monopile supported wind turbines in cohesive soil [J]. Soil Dynamics & Earthquake Engineering, 2013, 49(18):165-180.

[3] Bhattacharya S, Adhikari S. Experimental validation of soil–structure interaction of offshore wind turbines [J]. Soil Dynamics & Earthquake Engineering, 2011, 31(5):805-816.

[4] Bhattacharya S, Nikitas N, Alexander N A, et al. Observed dynamics soil-structure interaction in scale testing of offshore wind farm foundation [J]. Soil Dynamics & Earthquake Engineering, 2013.

[5] Arany L, Bhattacharya S, Macdonald J H G, et al. Closed form solution of Eigen frequency of monopile supported offshore wind turbines in deeper waters incorporating stiffness of substructure and SSI [J]. Soil Dynamics & Earthquake Engineering, 2016, 83:18-32.

[6] Arany L, Bhattacharya S, Adhikari S, et al. An analytical model to predict the natural frequency of offshore

wind turbines on three-spring flexible foundations using two different beam models [J]. Soil Dynamics & Earthquake Engineering, 2015, 74:40-45.
[7] Bhattacharya S, Lombardi D, Wood D M. Similitude relationships for physical modelling of monopile-supported offshore wind turbines [J]. International Journal of Physical Modelling in Geotechnics, 2011, 11(2):58-68.
[8] ISO 19901-4 (2016). Petroleum and natural gas industries-specific requirement for offshore structures. Part 4- geotechnical and foundation design considerations.
[9] Carswell W, Arwade S R, Degroot D J, et al. Soil–structure reliability of offshore wind turbine monopile foundations [J]. Wind Energy, 2015, 18(3):483-498.
[10] Harte M, Basu B, Nielsen S R K. Dynamic analysis of wind turbines including soil-structure interaction[J]. Engineering Structures, 2012, 45:509-518.
[11] Schafhirt S, Page A, Eiksund G R, et al. Influence of Soil Parameters on the Fatigue Lifetime of Offshore Wind Turbines with Monopile Support Structure [J]. Energy Procedia, 2016, 94:347-356.
[12] Bhattacharya S. Dynamics of wind turbines on two types of foundations [J]. Proceedings of the Institution of Civil Engineers Geotechnical Engineering, 2013, 166(2):159-169.
[13] Martakis P, Taeseri D, Chatzi E, et al. A centrifuge-based experimental verification of Soil-Structure Interaction effects[J]. Soil Dynamics and Earthquake Engineering, 2017, 103:1-14.
[14] Guo Z, Yu L, Wang L, et al. Model Tests on the Long-Term Dynamic Performance of Offshore Wind Turbines Founded on Monopiles in Sand [J]. Journal of Offshore Mechanics & Arctic Engineering, 2015, 137(4).
[15] Ahmed S S, Hawlader B. Numerical Analysis of Large-Diameter Monopiles in Dense Sand Supporting Offshore Wind Turbines [J]. International Journal of Geomechanics, 2016, 16(5):04016018.
[16] Carswell W, Arwade S R, Degroot D J, et al. Soil–structure reliability of offshore wind turbine monopile foundations [J]. Wind Energy, 2015, 18(3):483-498.
[17] Huang Y, Guo Z, Hong Y, et al. Investigations on Dynamic Responses of Offshore Wind Turbine Supported by Monopile in Sand[C]// Isope Pacific-Asia Offshore Mechanics Symposium, Pacoms. 2016.
[18] Abhinav K A, Saha N. Effect of scouring in sand on monopile-supported offshore wind turbines [J]. Marine Georesources & Geotechnology, 2016, 35(6).
[19] Corciulo S, Zanoli O, Pisanò F. Transient response of offshore wind turbines on monopiles in sand: role of cyclic hydro–mechanical soil behaviour [J]. Computers & Geotechnics, 2017, 83:221-238.
[20] Bisoi S, Haldar S. Dynamic analysis of offshore wind turbine in clay considering soil–monopile–tower interaction [J]. Soil Dynamics & Earthquake Engineering, 2014, 63(1):19-35.
[21] Tchakoua P, Wamkeue R, Ouhrouche M, et al. Wind Turbine Condition Monitoring: State-of-the-Art Review, New Trends, and Future Challenges [J]. Energies, 2014, 7(4):2595-2630.
[22] Weijtjens W, Verbelen T, De Sitter G, et al. Foundation structural health monitoring of an offshore wind turbine—A full-scale case study[J]. Structural Health Monitoring, 2016, 15(4): 389-402.
[23] Devriendt C, Magalhães F, Weijtjens W, et al. Structural health monitoring of offshore wind turbines using automated operational modal analysis[J]. Structural Health Monitoring, 2014, 13(6): 644-659.
[24] Swartz R A, Lynch J P, Zerbst S, et al. Structural monitoring of wind turbines using wireless sensor networks[J]. Smart structures and systems, 2010, 6(3), 183-196.
[25] Klis R, Chatzi E N. Data recovery via hybrid sensor networks for vibration monitoring of civil structures[J]. International Journal of Sustainable Materials and Structural Systems, 2015, 2(1-2): 161-184.
[26] Ashwini P, and Umamaherwari R. Wireless sensor network for condition monitoring of remote wind mill[C]// 2017 International Conference on Innovations in Green Energy and Healthcare Technologies (IGEHT). Coimbatore, 2017: 1-7.

[27] Schröder K, Gebhardt C G, Rolfes R. A two-step approach to damage localization at supporting structures of offshore wind turbines[J]. Structural Health Monitoring, 2018, 17(5): 1313-1330.
[28] Martinez-Luengo M, Kolios A, Wang L. Structural health monitoring of offshore wind turbines: A review through the Statistical Pattern Recognition Paradigm [J]. Renewable & Sustainable Energy Reviews, 2016, 64:91-105.
[29] Wang Y, Zhang T. Finite element model updating using estimation of distribution algorithm[C]//SHMII-6 2013: Proceedings of The 6th International Conference on Structural Health Monitoring of Intelligent Infrastructure. Hong Kong Polytechnic University, 2013: 1-8.
[30] Wang Y, Zhu X, Hao H, et al. Spectral element model updating for damage identification using clonal selection algorithm[J]. Advances in Structural Engineering, 2011, 14(5): 837-856.
[31] Welch P D. The use of fast Fourier transform for the estimation of power spectra: A method based on time averaging over short, modified periodograms [J]. IEEE Trans. Audio & Electroacoust, 1967, 15(2):70-73.
[32] Zierath J, Rosenow S E, Rachholz R, et al. Experimental Identification of Modal Parameters of a Wind Turbine and Comparison to Multibody Models[C] //DEWEK 2017: 13th German Wind Energy Conference. Bremen, 2017.
[33] Yahr G T. Fatigue Design Curves for 6061-T6 Aluminum[J]. Journal of Pressure Vessel Technology, 1997, 119(2):211-215.
[34] Larrañaga, P. and Lozano. Estimation of distribution algorithms: A new tool for evolutionary computation [M]. Kluwer Academic Publishers, 2001.
[35] Wang Y, Hao H. Damage identification scheme based on compressive sensing. Journal of Computing in Civil Engineering. 2013 May 9, 29(2):04014037.
[36] Wang, Y., Hao, H. and Peng, X.L., Simplified pipeline-soil interaction model for vibration-based damage detection of onshore pipelines. In ISSE11: Proceedings of International Symposium of Structural Engineering, 2010, pp. 1375-1380.